Natural Hazards
https://doi.org/10.1007/s11069-024-06916-3

ORIGINAL PAPER

Tsunami inundation limit based on probabilistic analysis of runup and inundation distance

Marilym Ramos[1,2] · **Rafael Aránguiz**[2,3] · **María Teresa Bull**[4]

Received: 19 March 2024 / Accepted: 5 September 2024

Abstract
Tsunamis are devastating natural hazards that can reach runups of 30 m in coastal areas. One of the most important mitigation measures to save human lives is evacuation, which requires identification of both the inundation area and safe zones. Currently, a ground elevation of 30 m is used to determine safe zones in Chile. However, it has also been used for urban planning, for which the actual tsunami hazard may be overestimated. This research aims to propose a criterion based on probabilistic analysis to determine the tsunami inundation limit, considering both the runup and inundation distance from the shoreline. To this end, a synthetic database of runup and inundation distance from the shoreline was analyzed. First, stochastic earthquake sources were used to simulate tsunami events up to an inundation level in 10 coastal cities. Second, maximum runup and inundation distance were calculated for each tsunami scenario along transect lines perpendicular to the coastline. Finally, three exceedance probabilities of runup – 0.5%, 1%, and 2% in 50 years – were calculated to estimate the runup and inundation distances for each city. The results showed that geomorphology has an important role in runup and inundation distance. In addition, this research introduced new criteria for inundation limit identification, which are more flexible and accurate than the current 30-m ground elevation criterion used for tsunami risk assessment and urban planning. The application of this proposed method would allow local authorities to improve the locations of both critical infrastructure and safe zones.

Keywords Tsunami · Chile · Runup · Inundation distance · Probabilistic hazard assessment · Numerical simulation

✉ Rafael Aránguiz
raranguiz@ucsc.cl

[1] Master programme in Civil Engineering, Universidad Católica de la Santísima Concepción, Concepción, Chile

[2] Department of Civil Engineering, Universidad Católica de la Santísima Concepción, Alonso de Ribera, Concepción 2850, Chile

[3] Research Center for Integrated Disaster Risk Management (CIGIDEN), Santiago, Chile

[4] Department of Industrial Engineering, Universidad Católica de la Santísima Concepción, Concepción, Chile

Published online: 12 September 2024

1 Introduction

Tsunamis, rare yet devastating natural hazards, are primarily triggered by submarine earthquakes, along with landslides and volcanic eruptions (Grezio et al., 2017). Recent tsunamis – such as the 2010 Chile tsunami, with a 29-m runup in Constitución; the 2004 Indian Ocean tsunami, which caused a 31-m runup in Lhoknga, Indonesia; and the 2011 Japan Earthquake, which resulted in a 39.7-m runup in Miyako City – exemplify the substantial coastal inundation caused by these events (Fritz et al. 2011; Borrero et al. 2006; Mori et al. 2011). These measurements align with historical tsunami records, such as the 20-25-m runup on Mocha Island due to the 1960 Chile tsunami (Takahashi 1961), the 38.2-m runup in the 1896 Meiji Sanriku tsunami, and the 28.7-m runup in the 1933 Showa Sanriku tsunami (Mori et al. 2011). To mitigate these risks, tsunami inundation maps have been developed, offering vital information for evacuation planning and long-term coastal development (Adriano et al. 2013; Cho et al. 2016; Grezio et al. 2017b; Naim et al. 2021). The tsunami inundation zone in Japan is defined by numerical simulation using a combination of worst-case scenarios. In addition, tsunamis are classified into two different levels: Level 1, more frequent events with low inundation depths, typically less than 7–10 m, and Level 2, rare events typically over 10 m, with inundation heights up to 20 and 30 m (Shibayama et al. 2013). In Peru, the tsunami inundation zone is also defined based on numerical simulations and is divided into two areas, one related to earthquakes of magnitude 8.5 Mw and a more extensive area related to earthquakes of magnitude 9.0 (CNAT 2021). In other cases, such as the city of Port Alberni, Canada, the tsunami inundation zone is defined as the area below 20 m.a.s.l. (Alberniweather 2005). In Chile, tsunami inundation maps are made by the Hydrographic and Oceanographic Service of Chilean Navy (SHOA for its name in Spanish) through numerical simulation of one extreme event. Although these maps are based on the worst-case scenario (Solís and Gazmuri 2017), in 2018 the National Service for Disaster Prevention and Response (SENAPRED and formerly ONEMI) developed a specific emergency plan that defined the 30-m.a.s.l. contour as a safe zone, following an international recommendation by the International Tsunami Information Center (IOC, 2014). This is consistent with results from Priest et al. (2010), who found through a probabilistic analysis that 99% of Cascadia tsunami variation is covered by runup $\leq$ 30 m.

The focus of both the inundation map and the 30-m.a.s.l. contour criterion in Chile is primarily on facilitating tsunami evacuation. However, due to the absence of other specific urban planning instruments such as probabilistic tsunami maps, the Ministry of Housing and Urbanism (MINVU) and the Ministry of Social Development (MDS) have indirectly advocated for the use of these tools in land-use planning for coastal cities. The MINVU is responsible for land-use planning, in collaboration with the municipalities of coastal cities through communal regulatory plans (CRPs). These CRPs are required to include risk areas related to various natural hazards. As a result, most municipalities use the available tsunami inundation maps (based on the worst-case scenario) as a hazard input (Álvarez et al. 2018). In 2017, the MDS introduced guidelines for project risk assessment (MDS 2017). According to these guidelines, if there is no CRP or it lacks tsunami hazard information or if there is no official inundation map, the 30-m contour criterion must be applied. Projects situated below this altitude are deemed to be at maximum risk (Martínez et al. 2017). As a consequence of this criterion, in many cases

risk-free areas are not available for the development of activities in the coastal zone. An illustrative case is the construction of the Constitución city hospital, for which SENAPRED recommended a location at least 30 m above sea level. This recommendation resulted in a decade-long delay in project approval and initiation (ONEMI, 2014; Jarpa 2015; Rey 2020; Orellana 2023). A similar scenario has unfolded with the Community Family Health Center (Cecof) in the town of Queule, stalled since 2017 due to the unavailability of land 30 m.a.s.l. This has led to a considerable increase in project costs due to the need for access routes (Ilustre Municipalidad Toltén 2017). While health services in coastal areas are advised to be located above 30 m.a.s.l., practical constraints such as a lack of land in certain areas at these elevations often pose challenges (Ministerio de Salud 2019; PUC, 2010). To resolve this issue, Vicuña and Schuster (2021) suggest that regulations consider risk in a graduated manner, correlating it with hazard levels, advocating for a more comprehensive risk mitigation analysis. An example of this approach can be seen in the CRP of Iquique, where risk is classified as "very high" for areas located below 10 m.a.s.l., "high" for areas between 10 and 20 m.a.s.l., "moderate" for areas between 20 and 25 m.a.s.l, and "low" for areas between 25 and 30 m.a.s.l. (Ilustre Municipalidad Iquique 2019).

The application of a criterion based on ground elevation only has an important disadvantage in that it does not consider the local behavior of tsunamis in coastal areas. It is known that coastal dunes and cliffs can act as natural barriers against tsunamis (Smart et al. 2016; Mikami et al. 2019; Widiyanto et al. 2020), while the existence of rivers, estuaries and coastal islands can affect the impacts of tsunamis since they cause channeling effects, increasing the inundation area (Reese et al. 2011; Shimozono et al. 2012). Moreover, Aránguiz and Catalán (2022) highlight the importance of considering the distance from shore and not only the ground elevation when defining the safe zone, especially in extensive low-lying areas where the 30-m elevation is located many kilometers inland. In fact, the runup of 31 m during the 2004 Indian Ocean tsunami refers to the maximum vertical excursion on the front of a small hill about 600 m off the shoreline (Synolakis and Kong 2006). In a similar manner, the 29-m runup due to 2010 Chile tsunami took place on a cliff located 120 m from the shoreline (Fritz et al. 2011). Moreover, Mori et al. (2011) analyzed the runup during the 2011 Japan Tsunami as a function of distance from the shoreline and found that runup decreased exponentially with increasing distance, up to 5 km from the shoreline.

In a previous work (Aranguiz et al., 2024), the authors developed probabilistic tsunami inundation maps for specific Chilean cities, utilizing a comprehensive tsunami source database and conducting a probabilistic hazard analysis. The present research focuses on a different aspect of tsunami hazards, specifically the probabilistic analysis of tsunami runup and inundation distance, to propose a more general and simplified criterion for determining the tsunami inundation limit. This will provide local communities without inundation maps or communal regulatory plans a tool to define safe zones and land use. The study focuses on ten coastal cities along the Chile-Peru subduction zone and uses numerical simulation of stochastic tsunami scenarios. Section 2 describes the methodology for generating, selecting and propagating tsunami scenarios, as well as generating the synthetic database for probabilistic analysis. The results are presented in Sect. 3, followed by a discussion in Sect. 4 and conclusion in Sect. 5.

2 Methodology

The first step in the probabilistic analysis is to gather a database of tsunami records. This is necessary for conducting a probabilistic analysis of tsunami runup and inundation distance. However, the current records available are not sufficient for a specific location. To overcome the limitations of available records, a synthetic database of tsunami runup is created using stochastic tsunami scenarios. This involves simulating hundreds of scenarios up to an inundation level in 10 coastal cities along the Chile-Peru subduction zone. This subduction zone is one of the most seismically active areas in the world. The tectonic environment of the region is characterized by the movement of the Nazca Plate beneath the South American Plate, which releases a significant amount of seismic energy globally (Barrientos 2018; León et al. 2019). Figure 1 provides a visual representation of the methodology, which consists of four consecutive steps. Step 0 is named as such because it serves as a starting point for the methodology, rather than being an integral part of it. The tsunami scenarios used in this study were proposed by Aránguiz et al. (2024). Step 1 involves conducting numerical simulations of tsunamis at all selected locations, while Step 2 entails selecting the runup and inundation distance for each scenario along multiple lines perpendicular to the coastline. This step essentially generates a synthetic runup-distance database. Finally, Step 3 involves the probabilistic analysis of this synthetic database, where the runup and inundation distance corresponding to a given exceedance probability are selected along each transect line. These four steps will be further explained in the following paragraphs.

In this study, we considered three tsunami hazard levels with exceedance probabilities of 0.5%, 1% and 2% over a 50-year lifetime, corresponding to 9,975, 4,975 and 2,475-year return periods, respectively. The Chilean tsunami design provisions,

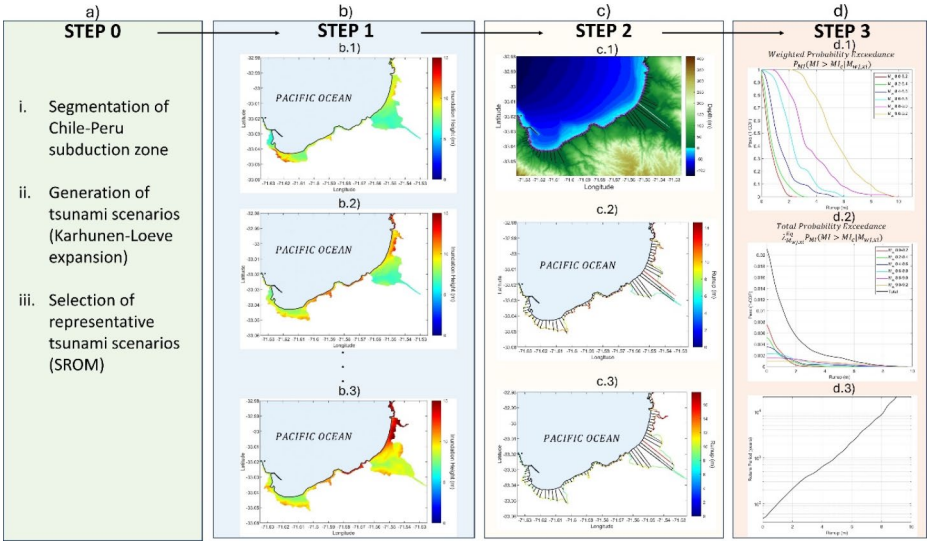

Fig. 1 Diagram of methodology. (**a**) Step 0: A review of starting point for the methodology. (**b**) Step 1: Examples of numerical simulations for Valparaíso – Viña del Mar. (**c**) Step 2: Examples of selecting the runup and inundation distance for each scenario along multiple transects perpendicular to the coastline. (**d**) Step 3: Probabilistic analysis of the synthetic database of runup and inundation distance

NCh3363:2015 (INN, 2015), do not specifically mention a design event, and it is assumed that the deterministic tsunami inundation map from SHOA (intended for evacuation) may be used. Therefore, the 2% in 50 years level is particularly relevant, as it aligns with the tsunami design criteria outlined in the ASCE 7–22 code (ASCE 2022), which sets this threshold as the design standard for coastal infrastructure to ensure resilience against extreme tsunami events. Additionally, it was observed that the 0.5% in 50 years level may approximate the conditions represented in current deterministic tsunami inundation maps of Chilean cities, while the 1% in 50 years represents an intermediate value for comparison. It is important to note that these tsunami hazard levels may differ from those used in seismic design. The return period of an earthquake cannot be directly translated to a return period of tsunami inundation. While an earthquake of a given magnitude may occur with a certain frequency, the resulting tsunami inundation is highly influenced by the earthquake's slip distribution, which can vary significantly for earthquakes of the same magnitude. As such, the return period for tsunami hazards reflects a combination of both seismic activity and the specific characteristics of individual tsunami events. On the other hand, seismic design considers a peak ground acceleration (PGA) with an exceedance probability of 10% in 50 years (475-year return period) as proposed in Eurocode 8, as well as the ASCE code before 1997 (Sukuoglu & Akkar, 2014). The basis of this design was to provide life safety under design ground motions. However, after 1997, the ASCE code´s design objective shifted to avoiding structural collapse under the maximum considered earthquake (MCE) ground motion, which corresponds to an exceedance probability of 2% in 50 years (2475-year return period). Regarding seismic design in Chile, NCh433.Of96 (INN 1996) determines seismic demand from a response spectrum, considering an allowable-design-level earthquake for broad seismic zones (Lagos et al. 2020). The design spectra are based on historical earthquake data, which provides a robust foundation for understanding and mitigating seismic risks (Massone 2013). Although these design events are based on historical earthquakes, new proposal have recently included performance-based design principles. For instance, in 2017, the Chilean Society of Seismology and Seismic Engineering (ASHISINA for its name in Spanish) proposed a method to include a Design-based earthquake (i.e. 475-year return period, or exceedance probability of 10% in 50 years) to ensure immediate occupancy after an event, and a Maximum Considered Event (i.e. 950-year return period or exceedance probability of ~5% in 50 years) to ensure life safety (Lagos et al. 2020). However, this proposal is not officially included in the seismic design code.

2.1 Step 0, Generation and selection of stochastic tsunami scenarios

The stochastic tsunami scenarios database is available in Aránguiz and Ramos (2024). The following paragraph provides a brief description of the methodology used in Aránguiz et al. (2024). The study area is presented in Fig. 2, which shows the latest and largest tsunamigenic earthquakes of magnitude $M_w \geq 8.0$ along the Chile-Perú subduction zone (Fig. 2a), as well as the 10 coastal cities selected for tsunami numerical simulations in the current study (red dots). Based on the characteristics of large earthquakes, a seismic segmentation was defined using the study of Saillard et al. (2017), which found that peninsulas act as barriers to earthquake rupture areas. As a result, the

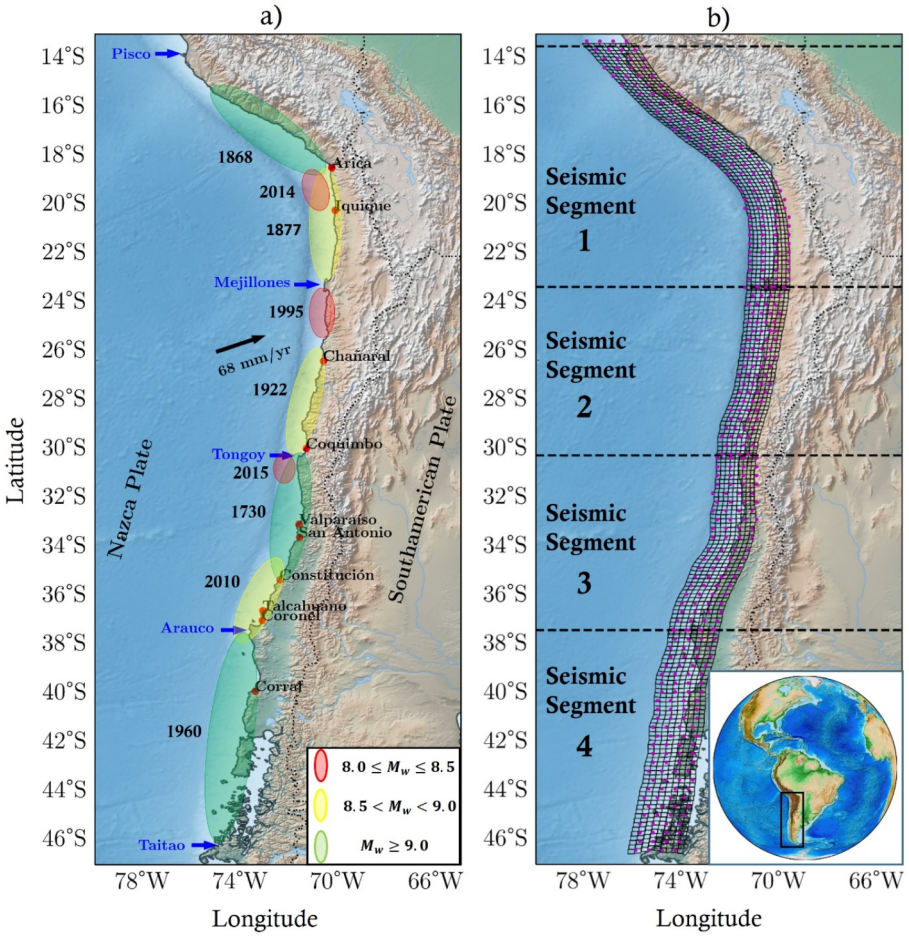

Fig. 2 Map of the study area. (**a**) Coastal cities considered for numerical simulations and main earthquakes $M_w \geq 8.0$ in the Peru-Chile subduction zone. (**b**) Seismic segments and fault geometry of the subduction zone divided into subfaults for the generation of stochastic earthquakes. Magenta points were used for the application of the SROM method. Modified from Aránguiz et al. (2024)

subduction zone was divided into four seismic segments, as shown in Fig. 2b. The first segment begins near Pisco, Peru, at the Nazca ridge, and ends at the Mejillones Peninsula, Chile. The second segment covers the area from the Mejillones Peninsula to the Tongoy Peninsula. The third segment begins at the Tongoy Peninsula and ends at the Arauco Peninsula, and the fourth segment runs from the Arauco Peninsula to the Taitao Peninsula in southern Chile. To create earthquake source models for each seismic segment, the Slab 2.0 model (Hayes et al. 2018) was utilized. This involved the generation of subfaults of approximately $20 \times 20 \text{km}^2$, as shown in Fig. 2b. The earthquakes with heterogeneous slip distributions were then generated using the Karhunen-Loeve (K-L) expansion (LeVeque et al. 2016). The minimum and maximum moment magnitudes considered for the synthetic earthquakes were as follows: M_w 8.0–9.2 for segments 1

and 3, M_w 8.0–9.0 for segment 2, and M_w 8.0–9.6 for segment 4. Each magnitude range was further divided into 0.2-magnitude bins.

The probabilistic analysis of tsunami inundation has a high computational cost, which increases as the grid resolution increases. Therefore, the Stochastic Reduced Order Model (SROM) was used (Grigoriu 2009). The SROM is a highly efficient tool for simulating various tsunami scenarios, significantly reducing the computational costs associated with uncertainty propagation. This model improves upon the traditional Monte Carlo method by incorporating two key steps: selecting a function sample and determining probabilities through an optimization process. In the work of Aránguiz et al. (2024), a target vector X was constructed using coseismic deformations, and statistical properties such as marginal distributions and correlation matrices were analyzed for each seismic segment and magnitude interval. This approach greatly enhances the precision of estimating tsunami-related uncertainties, while also being able to handle a substantial number of filtered scenarios ($n \sim 10{,}000$) with computational efficiency, as demonstrated by (Sepúlveda et al. 2017). In total, 50 earthquake scenarios were selected in each magnitude bin, resulting in a total of 300 scenarios for seismic segments 1 and 3, 250 scenarios for segment 2, and 400 scenarios for segment 4. It is important to note that in the optimization process the SROM method assigns a probability to each tsunami scenario; therefore, any probabilistic analysis should consider a weighted distribution function (Aránguiz et al. 2024). The weights used in this analysis are derived from coseismic displacements and are specific to individual magnitude bins according to the optimization process of the SROM method. To assess the stability of these weights, one would need to compare the results with a more localized analysis that uses different spatial areas and tsunami metrics. Although a full demonstration of this comparison is beyond the scope of this manuscript, a sensitivity analysis and comparison with traditional Montecarlo approach can be found in the work of Sepulveda et al. (2017).

2.2 Step 1, tsunami numerical simulations

The selected tsunami scenarios were simulated to an inundation level in several coastal cities. The following cities were chosen: Arica, Iquique, Chañaral, Coquimbo-La Serena, Valparaíso-Viña del Mar, San Antonio, Constitución, Talcahuano, Coronel, and Corral, as shown in Fig. 2a. These cities were selected due to their diverse morphologies, including large flat areas, as well as narrow river valleys with steep slopes. Tsunami numerical simulations were performed using the Non-hydrostatic Evolution of Ocean Wave (NEOWAVE) model (Yamazaki et al. 2011). Four nested grids were used in most locations except for Constitución and Corral, where five grids were used. Grids 1, 2, and 3 have resolutions of 120 arcsec (~3700 m), 30 arcsec (~900 m), and 6 arcsec (~180 m), respectively. Grids 4 and 5 have resolutions of 1 arcsec (~30 m) and 1/3 arcsec (~10 m). Grids 1 and 2 were built from the Global Bathymetric Model (GEBCO) and grid 3 was built from regional and local nautical charts, while grids 4 and 5 were built by combining nautical charts and additional local bathymetry provided by the DOP (Ports Works Division of the Ministry of Public Works). Similarly, the topography was collected from different sources, and Lidar data with a 2-m resolution is available for many cities (Aránguiz et al. 2024). Figures 3 and 4 show the highest-resolution grids of all selected cities. The simulations covered an elapsed time of 4 to 8 h to capture

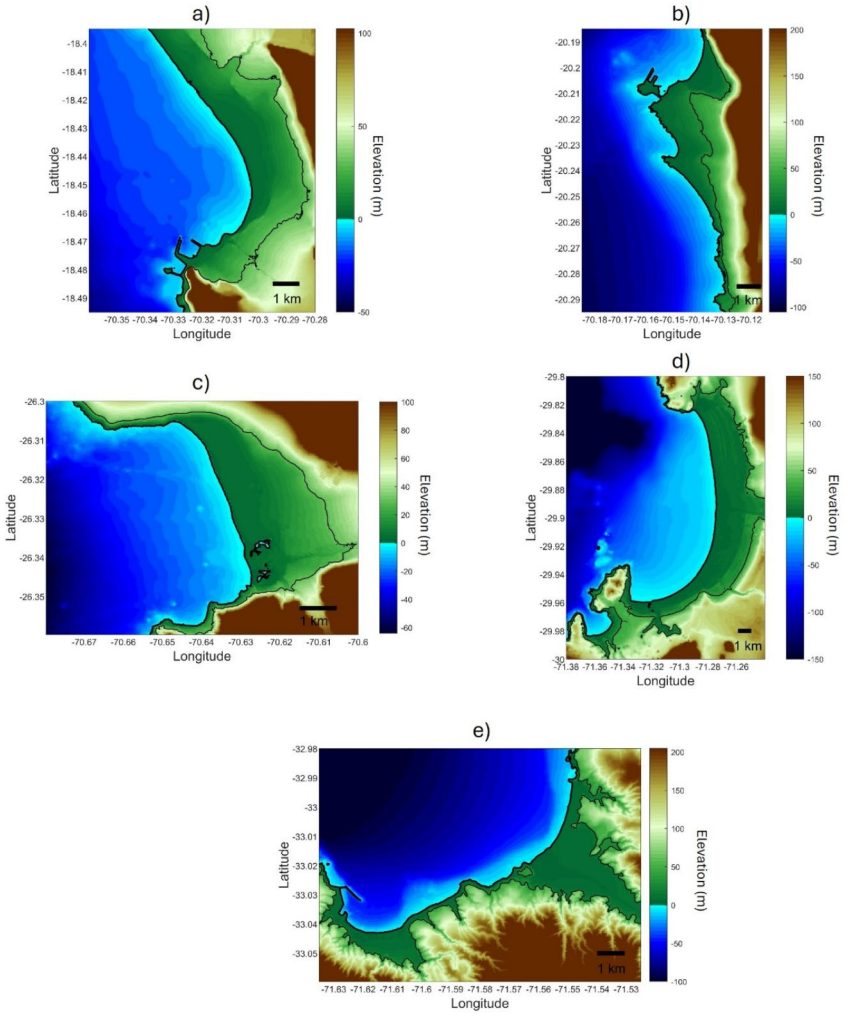

Fig. 3 Highest-resolution grids used in tsunami simulations of (**a**) Arica, (**b**) Iquique, (**c**) Chañaral, (**d**) Coquimbo – La Serena, (**e**) Valparaíso – Viña del Mar

the maximum amplitudes of tsunami waves from more distant scenarios, as well as the resonance effects in some cities such as Talcahuano, Arica, and Iquique (Aránguiz, et al., 2019; Cortés et al. 2017). The simulated tsunami scenarios for each city were those of the seismic segment where the city is located and the adjacent segments.

In the context of tsunami inundation simulations, surface roughness plays a crucial role in accurately modeling the interaction between tsunami waves and the coastal environment. For the simulations conducted in this study, the surface roughness coefficient is assumed to be constant, with a Manning's n value of 0.025. This value has been selected based on prior research and has been validated in studies such as Aránguiz et al. (2018), where it was shown to provide reliable results for similar coastal environ-

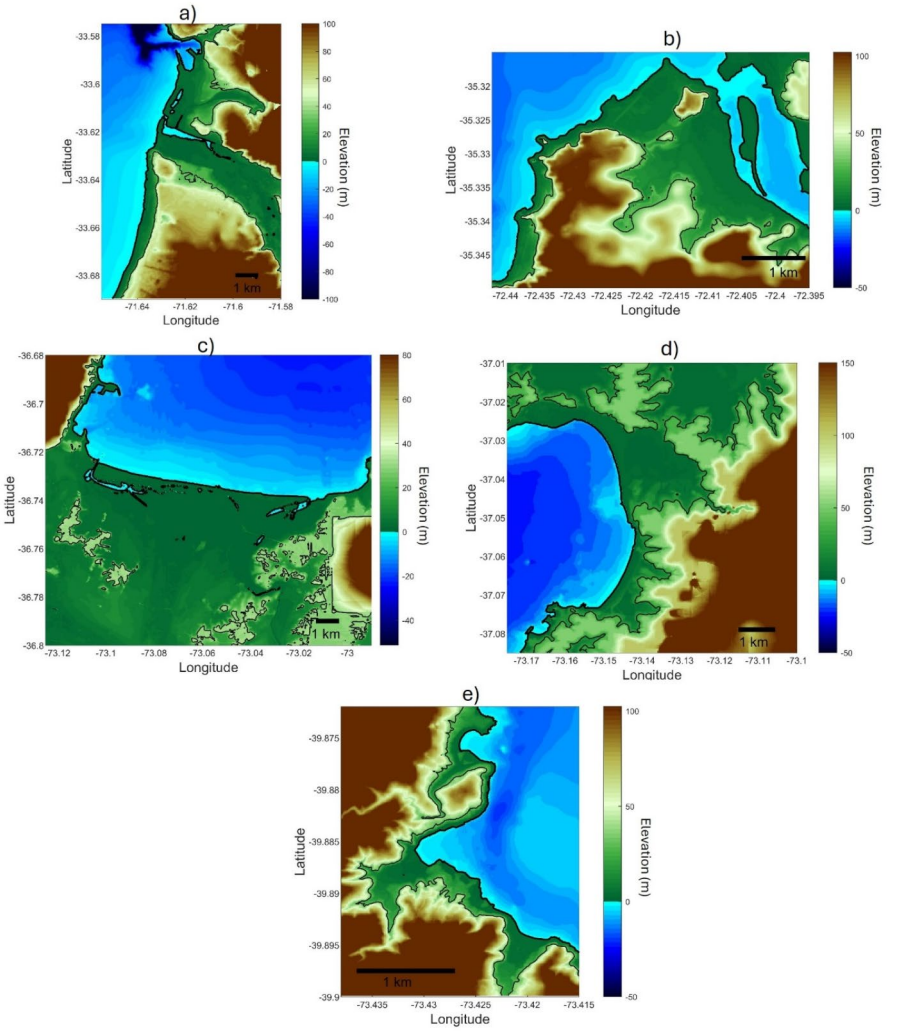

Fig. 4 Highest-resolution grids used in tsunami simulations of (**a**) San Antonio, (**b**) Constitución, (**c**) Talcahuano, (**d**) Coronel, (**e**) Corral

ments. The choice of a constant surface roughness coefficient simplifies the modeling process while still capturing the essential effects of frictional resistance on tsunami wave propagation and inundation. Although surface roughness can vary depending on specific local conditions, the use of a constant n value is a common and validated approach in tsunami modeling, providing a balance between computational efficiency and accuracy in simulating inundation dynamics.

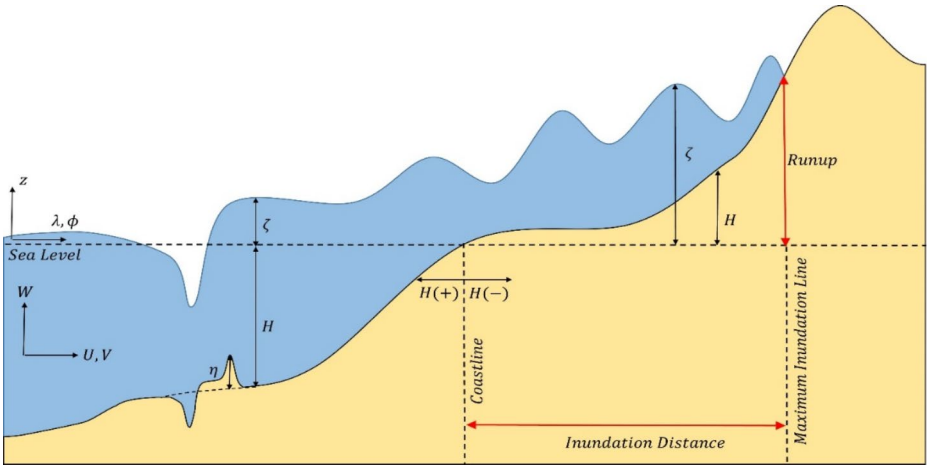

Fig. 5 Diagram of the free surface flow generated by the deformation of the seafloor in addition to the definition of variables for calculating runup (R) and inundation distance (D)

Table 1 Seismic parameters for calculation of annual recurrence (Aránguiz et al. 2024)

Seismic Segment	a_{eq}	b_{eq}	M_{max}
1	4.887	0.832	9.2
2	4.853	0.802	9.0
3	5.713	0.917	9.2
4	4.056	0.732	9.6

2.3 Step 2, generation of runup-distance database

The tsunami intensity measures considered were runup and inundation distance. Figure 5 illustrates the definition of runup (R), which is the maximum ground elevation flooded by the tsunami in relation to the sea level. Inundation distance (D) is the distance, measured perpendicularly to the coastline, to the points where the maximum inundation line is reached (UNESCO & IOC, 2019). To calculate inundation distance, the coastline of each city was divided into equal sections and then several transect lines (perpendicular to the coastlines) were drawn, as shown in the upper frame of Fig. 1c. The runup of each tsunami scenario was recorded along each transect line together with the distance from the shore, represented by the black dots in the middle and lower frames of Fig. 1c. The inundation distance was then computed along the transect line from the initial point (at the coastline) to the final point, where the runup occurs. This process was repeated for each coastal city and each simulated scenario. Therefore, a database of runup and inundation distance from shore was generated for each transect line, and a probabilistic analysis could be applied. Since the grids are expressed in geographical coordinates, it was possible to compute the distance using the haversine formula implemented in Matlab®. This equation is a special case of a more general formula (Eq. 1) of spherical trigonometry, the law of haversines, which relates the sides and angles of spherical triangles. It should be noted that this expression is an approxi-

mation when applied to the Earth because it is not perfectly spherical (Dauni et al. 2019; Prasetya et al. 2020).

$$hav\left(\frac{d}{r}\right) = hav\left(\varphi_2 - \varphi_1\right) + \cos\left(\varphi_1\right)\cos\left(\varphi_2\right) hav(\lambda_2 - \lambda_1) \tag{1}$$

Where hav is the haversine function: $hav\left(\theta\right) = \sin^2\left(\frac{\theta}{2}\right) = \frac{1-\cos(\theta)}{2}$, d is the spherical distance between two points, r is the radius of the sphere, in this case the radius of the Earth, φ_1, φ_2 the latitude of point 1 and latitude of point 2, and λ_1, λ_2 the longitude of point 1 and longitude of point 2. Solving Eq. (1) allows the inundation distance from the coastline to be obtained for the maximum inundation lines of each scenario. The length of equal sections along the shoreline varied according to the size of the coastal city under study; for instance, it was 50 m in Corral, 150 m in Constitución, 200 m in Chañaral and Valparaíso, 250 m in Arica, Iquique and San Antonio, 300 m in Coronel, 350 m in Coquimbo, and 600 m in Talcahuano. In Corral and Constitución, the distances are smaller because the highest-resolution grids are smaller, while in Talcahuano, the grid size is the largest.

The NEOWAVE numerical model calculates the total depth of water $D_{j,k}^m$ in the cell (j,k) and at time step m using the following expression:

$$D_{j,k}^m = \zeta_{j,k}^m + H_{j,k}^m - \eta_{j,k}^m \tag{2}$$

Where $\zeta_{j,k}^m$ is the water elevation from mean sea level, $H_{j,k}^m$ is the terrain height considering mean sea level as a reference (corresponding to grid height), and $\eta_{j,k}^m$ is the deformation of the ocean floor calculated with the method of Okada (1985). The sign convention that NEOWAVE uses for height $H_{j,k}^m$, is positive to the left and negative to the right of the coastline (Fig. 2). Water elevation $\zeta_{j,k}^m$ is calculated in the entire computational domain by integrating the momentum and continuity equations with the implicit non-hydrostatic pressure solution presented in Yamazaki et al. (2011). These equations allow us to calculate $\zeta_{j,k}^m$ in the center of the cell (j,k) of the grid in terms of the fluxes in x and y, FLX and FLY, from:

$$\zeta_{j,k}^{m+1} = \zeta_{j,k}^m + \left(\eta_{j,k}^{m+1} - \eta_{j,k}^m\right) - \Delta t \frac{FLX_{j+1,k} - FLX_{j,k}}{R\Delta\lambda\cos\phi_k} \tag{3}$$

Where Δt is the time step size, $\Delta\lambda$ is the grid size along the longitude coordinate, R is the radius of the earth, and ϕ_k is the latitude coordinate of the cell. The terms FLX and FLY in the cell (j,k) are calculated by:

$$FLX_{j,k} = U_p^{m+1}\zeta_{j-1,k}^m + U_n^{m+1}\zeta_{j,k}^m + U_{j,k}^{m+1}\frac{\left(H_{j-1,k} - \eta_{j-1,k}^m\right) + \left(H_{j,k} - \eta_{j,k}^m\right)}{2} \tag{4}$$

$$FLY_{j,k} = V_p^{m+1}\zeta_{j,k}^m + V_n^{m+1}\zeta_{j,k+1}^m + V_{j,k}^{m+1}\frac{\left(H_{j,k} - \eta_{j,k}^m\right) + \left(H_{j,k+1} - \eta_{j,k+1}^m\right)}{2} \tag{5}$$

Where U and V are the depth-averaged velocity components and the subscripts p and n indicate upwind and downwind velocity:

$$U_p^m = \frac{U_{j,k}^m + \left|U_{j,k}^m\right|}{2},\ U_n^m = \frac{U_{j,k}^m - \left|U_{j,k}^m\right|}{2},\ V_p^m = \frac{V_{j,k}^m + \left|V_{j,k}^m\right|}{2},\ V_n^m = \frac{V_{j,k}^m - \left|V_{j,k}^m\right|}{2} \quad (6)$$

For the runup calculation, it is necessary to describe the retreat of the inundation line as well as the water depth by updating the dry cells. To this end, a marker $CELL_{j,k}^m$, updates cell status based on water depth. If $D_{j,k}^m$ is positive, the cell is under water and $CELL_{j,k}^m = 1$, and if $D_{j,k}^m$ is zero or negative, the cell is dry and $CELL_{j,k}^m = 0$. The inundation line retreat procedure is repeated to update the dry-wet interface for each time step m. Therefore, the runup will be equal to $\zeta_{j,k}^m$ at the point where $D_{j,k}^m$ is zero. The lower frames of Fig. 1-c illustrate inundation limits as a function of the runup for two examples of tsunami scenarios.

2.4 Step 3, probabilistic analysis of the synthetic database

Once the runup and inundation distance database is generated, it is possible to compute the joint average return period by combining the seismic recurrence with the exceedance probability of the tsunami intensity measure MI (Sepúlveda et al. 2019), as follows:

$$T_R\left(MI_c\right) = \frac{1}{\sum_j \sum_i \lambda_{M'_{wj,x_i}}^{Eq} P_{MI}(MI > MI_c | M'_{wj,x_i})} \quad (7)$$

Where $\lambda_{M'_{wj,x_i}}^{Eq}$ is the average annual exceedance rate of earthquakes of magnitudes within the interval M'_{wj} in the seismic segment x_i, calculated using the truncated Gutenberg Richter Law (Kramer 2014):

$$\lambda_{M'_{wj,x_i}}^{Eq} = \nu \frac{e^{-\beta\left(m - M_{min}\right)} - e^{-\beta\left(M_{max} - M_{min}\right)}}{1 - e^{-\beta\left(M_{max} - M_{min}\right)}} \quad (8)$$

$$M_{min} \leq\ m \leq\ M_{max}$$

Parameter $\nu = \exp(\alpha - \beta\, M_{min})$, along with $\alpha = 2.303 a_{eq}$ and $\beta = 2.303 b_{eq}$, is a seismic parameter calculated for the corresponding seismic segment of Fig. 2-b (Aránguiz et al. 2024). The minimum magnitude was $M_{min} = 5.0$, while the maximum magnitude depended on the seismic segment. The term $P_{MI}(MI > MI_c | M'_{wj,x_i})$ is the exceedance probability of tsunami intensity measure MI being exceeded given an earthquake within the interval M'_{wj} in the seismic segment x_i. This exceedance probability is calculated using the empirical weighted cumulative distribution function with the weights obtained from the application of the SROM method in the selection of tsunami scenarios. Examples of exceedance probability curves of one transect line for several magnitude intervals are shown in the upper frame in Fig. 1d. The middle frame shows the same exceedance probability curves combined with average annual exceedance rate of earthquakes. Finally, in Fig. 1d, the lower frame shows the return period of runup for a given transect line.

To use the results for structural design requirements and urban planning, the following expression was considered in the calculation of return periods associated with the probability that an intensity measure will be exceeded within the lifetime of a structure:

$$P = 1 - (1 - 1/T_R)^L \tag{9}$$

Considering a lifetime L =50 years and three exceedance probabilities, P,: 0.5, 1, and 2%, three return periods may be calculated T_R: 9975, 4975, and 2475 years.

3 Results

The following paragraphs show the results of the probabilistic analysis of tsunami runup and inundation distance. The results are displayed for each city, with a line made up of points associated with their respective transects and a color scale to identify the runup. In addition, cities are displayed as a function of geographical location from north to south.

Figure 6 displays the inundation limit as a function of runup in the cities of Arica, Iquique, and Chañaral. The thick black line represents the coastline, while the thin black line represents the 30-m.a.s.l. contour as a reference. The shape of the runup line is consistent for each probability. However, as the probability decreases, both the runup value and maximum inundation distance increase. For instance, at a probability of 2% in 50 years, the maximum runup is 8 m in Arica and Iquique and 13 m in Chañaral. In comparison, at a probability of 0.5% in 50 years, the maximum runup reaches 14 m, 13 m, and 19 m in Arica, Iquique, and Chañaral, respectively. Similarly, the inundation distance also increases as the exceedance probability decreases, with values ranging from 1300 m to 1600 m in Arica, from 750 m to 1030 m in Iquique, and from 1190 m to 1390 m in Chañaral. These results are consistent with previous events in the region. The 1868 and 1877 earthquakes, each with an estimated magnitude of 8.8 (See Fig. 2), resulted in tsunami heights of 18 m and 9 m in Arica, respectively. In Iquique, maximum inundation heights were 12 m and 6 m for the same events (NCEI & WDS, 2023). The most recent event occurred in 2014 (M_w 8.2), causing a tsunami with an inundation distance of 100 m and a maximum runup of 2.5 m in Playa Cavancha, Iquique. Meanwhile, in Arica, the highest runup was 2.76 m in a rocky area south of the city's port (Catalán et al. 2015). In Chañaral, the last major event was in 1922, and historical records indicate that the tsunami reached a height of 10 m one hour after the earthquake (Cubelos et al. 2019).

It is important to note that the probabilistic inundation limits of cities are strongly influenced by their topography. For example, Arica is situated at the bend where the coast of South America abruptly changes direction. The continental shelf in this area is characterized by a nearly uniform slope and depth range of 0 to 200 m, with a relatively constant width (Cortés et al. 2017). Iquique is located on a relatively straight coast, with a wide continental shelf. In addition, both cities have steep slopes on their eastern edges, resulting in an elevation of approximately 25 to 30 m.a.s.l. a short distance from the coastline (León et al. 2019). According to Cortés et al. (2017) the bathymetry of Arica and Iquique is characterized by a uniform shelf, which can enhance tsunami resonance conditions. This highlights the significant impact of morphological characteristics on the tsunami response. In contrast, the town of Chañaral has a sandy beach with a gentle slope, with only the northern and southern areas of the bay having steeper slopes. Therefore, it is observed that the inundation limit presents abrupt changes in

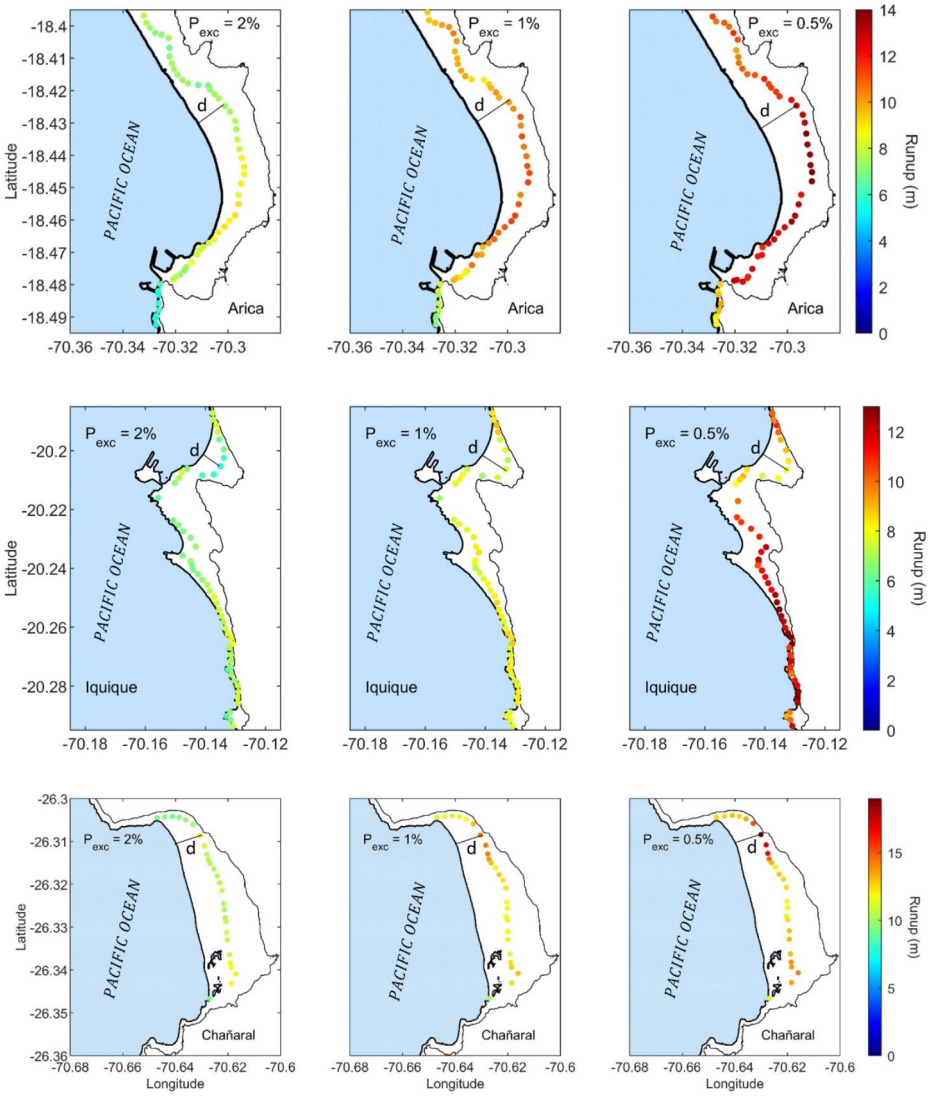

Fig. 6 Inundation line as a function of runup value associated with exceedance probabilities of 2, 1, and 0.5% in 50 years for Arica, Iquique, and Chañaral

runup value short distances from the shoreline. However, in Arica and Chañaral, it is also observed that the runup increases as a function of the inundation distance. To illustrate this, Fig. 7 shows the slope maps of these two locations. It can be seen that due to the topography, the water is channeled inward due to strong changes in slope, resulting in runup values of 14 m at long distances of approximately 1600 m in Arica and 19 m at distances of almost 900 m in Chañaral.

Figure 8 shows the results of the inundation limit as a function of runup for Coquimbo - La Serena, Valparaíso - Viña del Mar, and San Antonio. In the Coquimbo - La

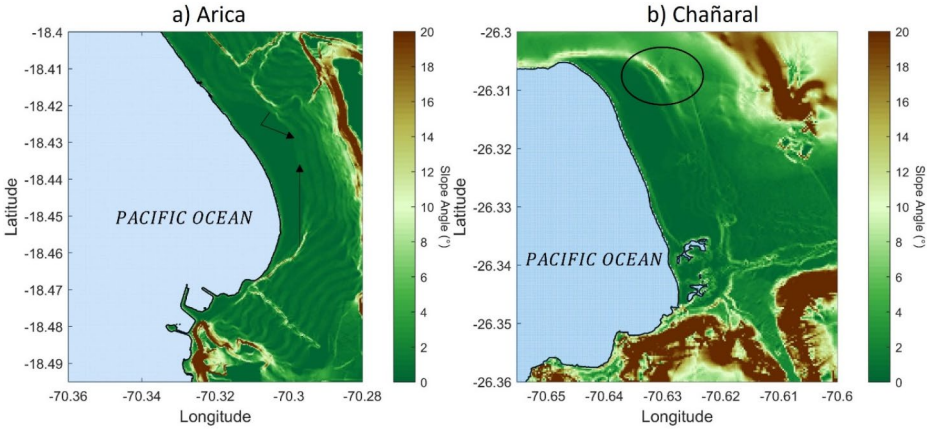

Fig. 7 Slope map for the cities of (**a**) Arica, and (**b**) Chañaral

Serena area, the maximum runup can reach 5 m in the northern and central parts of the bay, while in the southern area, it can reach 15 m for the lowest exceedance probability. The change in inundation distance is minimal between 2% and 0.5% probability of exceedance, and the maximum inundation distance remains constant at approximately 1500 m. The most recent tsunami event in this area occurred in 2015, with a maximum runup of 6.41 m in the southern area of the bay, and only 2.98 m in the central part. The maximum inundation distance was 700 m inland (Aránguiz et al. 2016). Similarly, in 1922, another event generated a wave height of 7 m in the southern area of the bay (NCEI & WDS, 2023). Coquimbo Bay has a flat, low-lying topography with a sandy beach and a 10-km-wide shelf. The seafloor has a gentle slope, and depths within the bay do not exceed 50 m (Aránguiz et al. 2016). Additionally, the cities in this area have a network of coastal wetlands that act as a buffer zone against tsunami impact. In fact, areas behind the wetlands experienced less flooding during the 2015 event (Van Den Berg et al. 2016).

In the Valparaiso-Viña del Mar conurbation (Fig. 8, central panels), runups of 9 to 15 m are observed in cliff-lined areas, while the flat zones experience smaller runups, ranging from 5 to 8 m depending on the exceedance probability. Additionally, it has been noted that the inundation distance can reach up to 1100 and 1670 m in low-laying areas as the exceedance probability decreases, but it remains below 200 m in cliff-lined areas. This is not unexpected, as elevated coasts are less vulnerable to large inundations compared to flat coasts where large floods are more common, since the water does not encounter resistance (Charvet et al. 2013), and Valparaíso and Viña del Mar are cities located on coastal plains flanked by several hills (León et al. 2019). The results are consistent with records from the last major earthquake and tsunami in 1730 (See Fig. 2), when the maximum runup reached 11 m.a.s.l. and the inundation distance reached 850 m (Carvajal et al. 2017). The 2015 event was also recorded on area beaches, with runups of 3 m and inundation distances of less than 20 m. A similar situation is observed in San Antonio (Fig. 8, lower panels). This city is characterized by cliff-lined coasts in both the southern and northern areas of the Maipo River mouth. Maximum runups range from 11 to 14 m along the coastal cliffs, while in the flat area they range between just 4.5 and 5.5 m, depending on the probability. The maximum

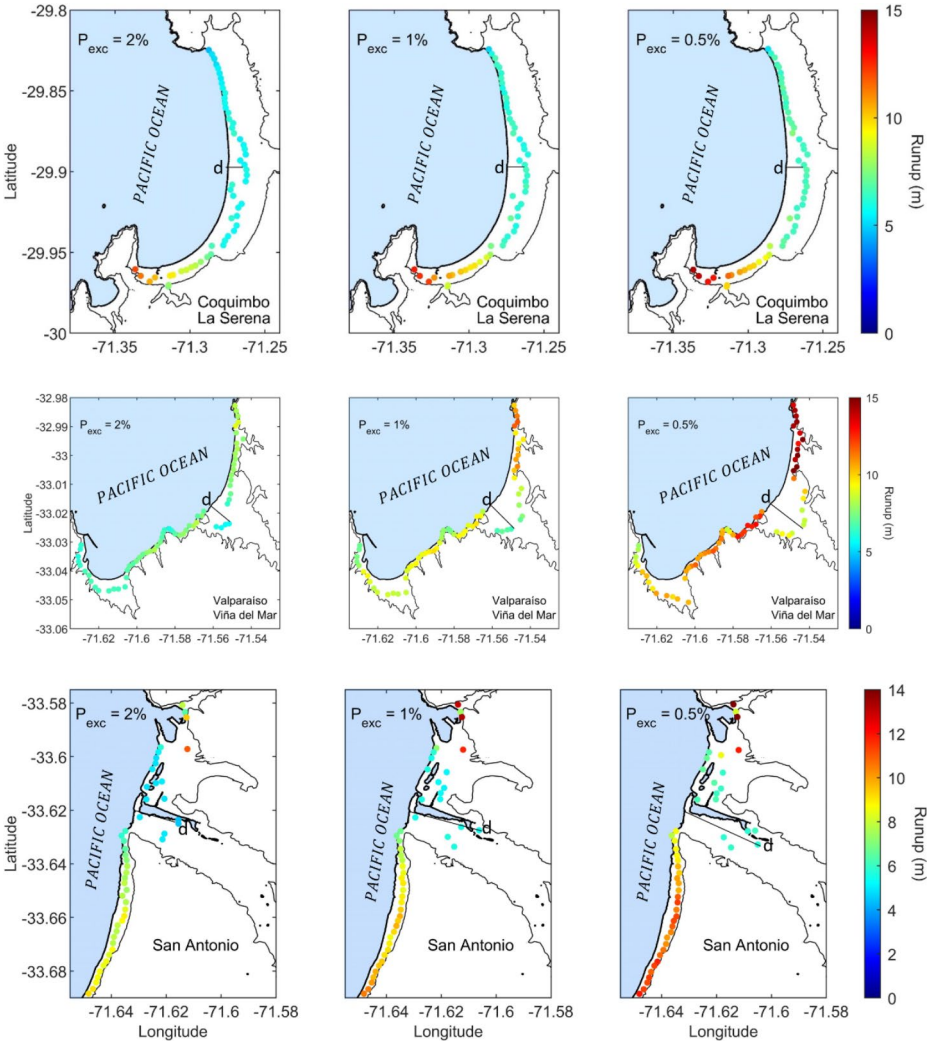

Fig. 8 Inundation line as a function of runup value associated with exceedance probabilities of 2, 1, and 0.5% in 50 years for Coquimbo – La Serena, Valparaíso – Viña del Mar, and San Antonio

inundation distance ranges from 1600 to 2900 m due to the tsunami surging into the Maipo River. It is important to mention that San Antonio is located in front of a submarine canyon, which may reduce the impact of tsunamis (Aranguiz and Shibayama 2013). The city reported a tsunami amplitude of only 2 m inside the port and 1-m flow depth at the container terminal in the southern part of the port during the 2010 tsunami.

Figure 9 illustrates the relationship between inundation limit and runup in the cities of Constitución, Talcahuano, and Coronel. In the case of Constitución, the cliff area facing the Pacific Ocean experiences the highest runups, ranging from 10 to 15 m, with maximum distances of 50 to 150 m as the probability of exceedance decreases. North of the cliff area, there is a flat area exposed to the sea, in which inundation distances reach 300 m and

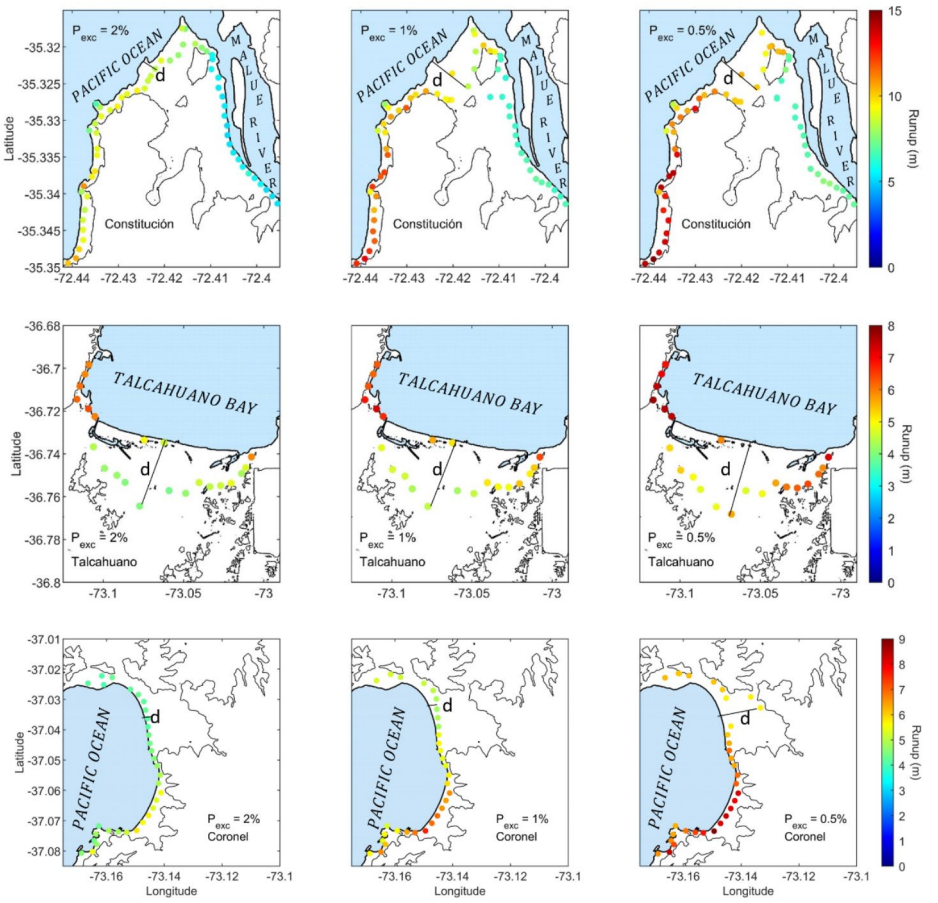

Fig. 9 Inundation line as a function of runup value associated with exceedance probabilities of 2, 1, and 0.5% 50 years for Constitución, Talcahuano, and Coronel

runup reaches 7 m for the 2% exceedance probability in 50 years. The runup can increase to 9 and 10 m for the exceedance probabilities of 1 and 0.5%, respectively, with an inundation distance of 800 m in both cases. Along the Maule River, the runup remains between 5 and 6 m for all exceedance probabilities, while the inundation distance ranges from 100 to 500 m. These results are consistent with records from the last major event in 2010, where the maximum runup was 29 m along the cliff-lined coast, with an inundation distance of 120 m from the shoreline. Similarly, smaller runup measurements were observed in the city center, located along the Maule River, with an inundation distance of approximately 500 m (Fritz et al. 2011).

In Fig. 9, the middle row displays the results for Talcahuano, showing that there are no significant differences in the inundation area as the exceedance probability increases. In the cliff-lined areas, the runup can reach 8 m, while flat areas experience an inundation distance of 4 km with a runup of approximately of 5 m for the lowest exceedance probability. The topography of Talcahuano plays a crucial role in the extent of tsunami inundation. The

southern shore of the bay consists of a coastal plain with a terrain elevation ranging from 5 to 10 m, bordered by hills with heights ranging from 50 to 130 m (León and March 2014). In addition, the bay faces north and has a relatively rectangular shape, measuring 14 km in length and 11 km in width, with a maximum water depth of 30 to 40 m at the entrance. Furthermore, the area is characterized by wetlands that are divided by a network of channels influenced by tides, forming a drainage system parallel to the coast, which serves as a channel for water (Morton et al. 2011). Historical records indicate that the 1730 tsunami reached a runup of 8 m and even flooded areas located 9 m.a.s.l. and 350 m from the coastline (Carvajal et al. 2017). In addition, the 1960 tsunami had a wave height of 5 m at the southern shore of the bay, resulting in limited inundation distance (NCEI & WDS, 2023). By contrast, the third and largest wave of the 2010 tsunami flooded a large area of the city, with a maximum runup of 8 m and an inundation distance up to 4 km (Fritz et al. 2011).

Coronel Bay presents a relatively limited tsunami impact. However, the southern shore behaves differently compared to the northern area. The former experiences runups ranging from 5 to 9 m and a limited distance, while the latter has runups of 5 to 6 m and an inundation distance of 500 to 1200 m, depending on the exceedance probability. During the 2010 tsunami, Coronel experienced limited inundation, with the maximum runup of 2.5 m in the southern part of the bay. This can be attributed to the presence of the Biobio submarine canyon (Aranguiz and Shibayama 2013), which causes tsunami waves to refract and change direction. This effect is further enhanced by diffraction from Santa Maria Island.

Figure 10 shows the results of inundation as a function of runup for Corral. While the extent of the inundation area does not visibly vary with the defined exceedance probability, there is a significant change in runup values in the flat areas, from 8 m to 14 m. This can be attributed to the fact that during the inundation, some of the kinetic energy of the tsunami is converted into potential energy. In cases where there is a sudden change in slope, a large amount of energy is transformed into potential energy (Ogami and Sugai 2018). These results are consistent with the inundation in 1960, when an inundation height of 10 m was recorded.

Figure 11 shows the relationship between runup and inundation distance. Figure 11a displays all pairs of runup-distance data and for all transect lines in all locations. It can be seen that maximum runups can easily exceed 25 m and even 30 m in some locations. In general, the maximum runup decreases as distance from the shoreline increases. Special cases are

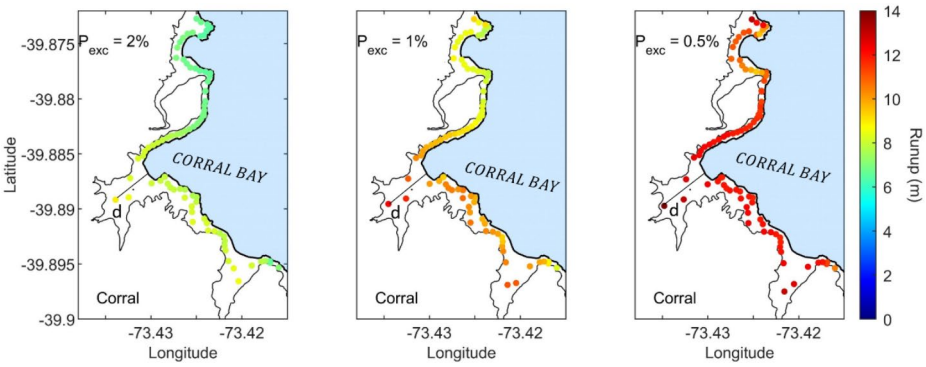

Fig. 10 Inundation line as a function of runup value associated with exceedance probabilities of 2, 1, and 0.5% in 50 years for Corral

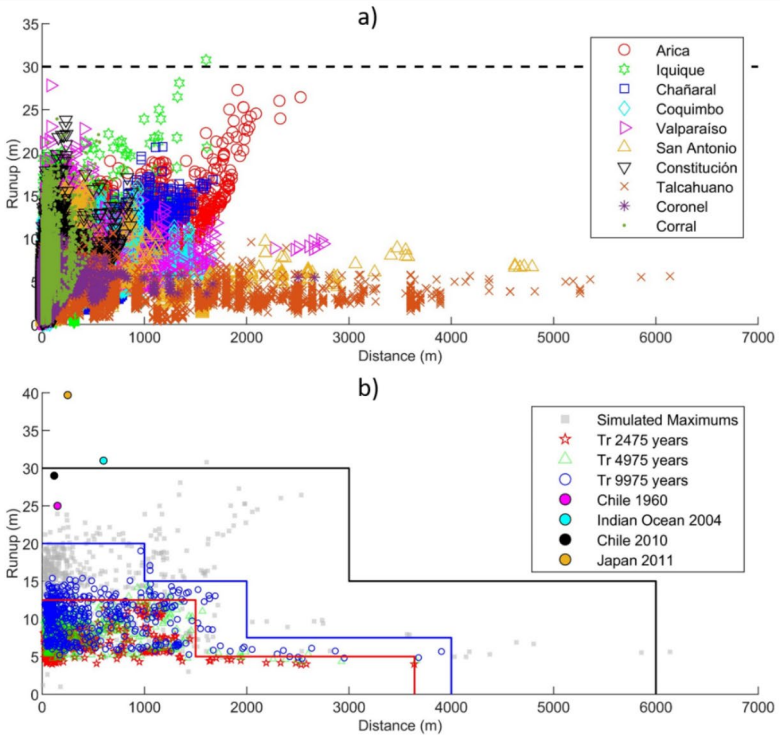

Fig. 11 (**a**) Runup and inundation distance measurements for all locations, transects, and simulated scenarios. (**b**) Runup and inundation distance measurements associated with return periods of 2470, 4975, and 9975 years, along with historical maximum measurements and simulated scenarios for all locations

Arica and Iquique, where the runup values increase with increasing distance, which is due to the geomorphology, which channels water and causes large runups inland where steep slopes are located. This behavior also occurs to a lesser extent in Chañaral, where high runups are generated in areas where the inundation distance is long. The rest of the localities present a behavior similar to that of Constitución, where cliff areas are characterized by large runups and distances less than 500 m, while flat areas are characterized by small runups and long distances. It is worth noting the results in Talcahuano, where the inundation distance can reach 6 km inland. Meanwhile, Fig. 11b shows the probabilistic results associated with three return periods in all locations, namely: 2475, 4975, and 9975 years (or 2, 1 and 0.5% probability of exceedance in 50 years). For comparison, the maximum simulated points of each transect line (light grey) and historical data (solid circles) are also shown. Based on these results, several criteria can be proposed. The first criterion can be defined as an envelope of maximum runups, which may be used for planning tsunami evacuation and the locations of safe zones, as illustrated by the black line in Fig. 11b. In this case, the first area is defined by the 30-m contour line from the shoreline to 3 km inland. Then, the second area is defined by the 15-m contour line between 3 and 6 km inland, and finally, areas further than 6 km inland may be considered safe from tsunami inundation. The second criterion is based on probabilistic results, such as the blue line in Fig. 11b. This line corresponds to an envelope of runup with a 0.5% probability of exceedance in 50 years (9975-year return

period). In this case, the 20-m contour may be used from the shoreline to 1 km inland, followed by the 15-m contour from 1 to 2 km inland, and then the 7.5-m contour from 2 to 4 km inland, while the area beyond 4 km may be considered safe from tsunami inundation. This criterion could be used for urban planning and the location of critical infrastructure, as a tsunami has a very low probability of exceeding this limit. The third criterion could be defined for structural design of public and private infrastructure (red line in Fig. 11b), which is based on the 2% probability of exceedance in 50 years (return period of 2500 years). The limit may be defined as the 12.5-m ground elevation from the shoreline up to 1.5 km inland, followed by 5 m from 1.5 to 3.5 km, while structures located further than 3.5 km from the shoreline do not need to be designed to withstand tsunami forces. As expected, the results related to the 1% exceedance probability in 50 years (4975-year return period) are between those of the two previous exceedance probabilities, but no significant differences are observed. Therefore, only two criteria based on probabilistic analysis are suggested.

Figure 12 shows an application of the previously presented probabilistic criteria to the city of Viña del Mar, as well as a comparison with fully probabilistic tsunami inundation maps. Figures 12a and c show a spatial representation of probabilistic criteria that could be used for urban planning (blue line in Fig. 11b) and structural design requirements (red line in Fig. 11b), respectively. The 30-m contour level is also shown in the figure as a solid black line. Figures 12b and d show the probabilistic maps obtained by Aránguiz et al. (2024), corresponding to exceedance probabilities of 0.5% and 2% for the same location. It can be seen that the criterion based on probabilistic analysis of runup with a 0.5% exceedance probability (Fig. 12a) presents an inundation area similar to that of the fully probabilistic map in the area less than 1 km from the shoreline. However, in the zone between 1 and 2 km from the shoreline, the inundation area is slightly overestimated compared to the probabilistic map. Beyond 2 km from the shoreline, the proposed criterion would slightly underestimate the inundation. In the case of the criterion based on runup with a 2% exceedance probability (Fig. 12c), which may be used for structural design requirements, the inundation area is overestimated compared to the fully probabilistic map in the area less than 1.5 km from the shoreline. Beyond that distance, the inundation is slightly underestimated. This comparison confirms that the proposed criteria align with fully probabilistic maps. Moreover, the currently proposed method is much less expensive in computational terms than the probabilistic maps. Therefore, coastal communities could use the proposed criteria if no official inundation maps are available. Finally, comparison of the simplified proposed criteria and the fully probabilistic maps to the 30-m ground elevation criterion (solid black line) for the location of critical infrastructure or structural design requirements for buildings shows that latter would be very restrictive. Therefore, it is recommended to use either of the two proposed criteria for urban planning and maintain the 30-m ground elevation criterion for evacuation purposes only.

4 Discussion

Estimating tsunami probabilities based on recorded data is feasible at a regional scale, as seen in Kulikov et al. (2005), who estimated runups of 13 m and 25 m for 50-year and 100-year return periods along southern Peru and northern Chile. However, establishing probabilities for specific locations is challenging due to the limited event catalog that matches

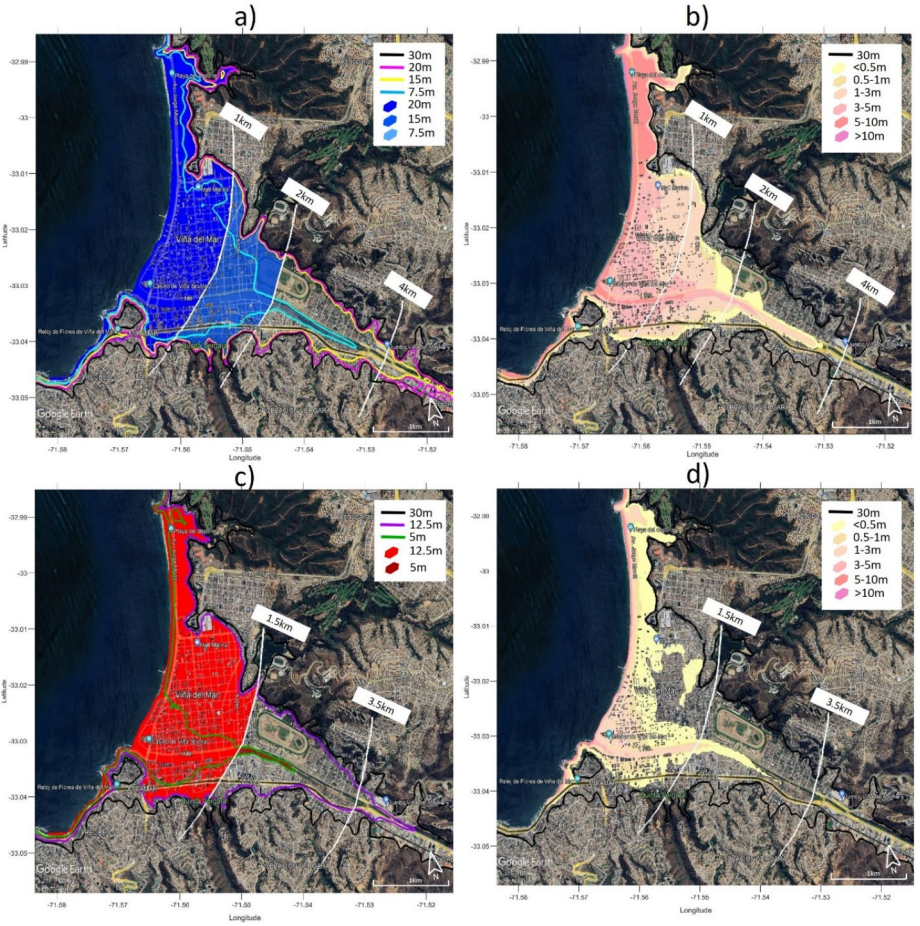

Fig. 12 Comparison of criteria based on probabilistic analysis and probabilistic inundation maps for the city of Viña del Mar. (**a**) Urban planning probabilistic criterion (blue line Fig. 11b). (**b**) Probabilistic inundation map associated with 0.5% exceedance probability in 50 years (Aránguiz et al. 2024). (**c**) Structural design probabilistic criterion (red line in Fig. 11b). (**d**) Probabilistic inundation map associated with 2% exceedance probability in 50 years (Aránguiz et al. 2024)

desired risk tolerances (Geist and Parsons 2006). Therefore, this study employed a computational approach to create a synthetic database of tsunami runup and inundation distances. This method allows for a more nuanced analysis by considering multiple points across an area and incorporating slip distribution uncertainties and potential earthquake locations (Sepúlveda et al. 2017, 2019). The findings extend our understanding of tsunami hazards by providing detailed runup-distance data along the Chile-Peru subduction zone.

Coastal areas, often settled for housing, maritime facilities, and tourism, require careful tsunami hazard management. Applying a uniform 30-meter elevation as an inundation limit may be overly conservative, especially given Chile's complex coastal morphology (Yamazaki and Cheung 2011; Aránguiz & Shibayama, 2013). This study underscores the importance of local geography and topography in defining safe zones. For instance,

coastal dunes, cliffs, and rivers can serve as natural barriers against tsunamis (Aránguiz and Catalán 2022). Incorporating distance from the shore along with tsunami runup provides a more accurate assessment of local tsunami behavior, with higher runup elevations on steep slopes and lower elevations on wide, flat beaches. This aligns with field data from Mori et al. (2011), showing an exponential decrease in runup with increased distance from shore. Therefore, elevation-based criteria alone may not be ideal for urban planning (Grezio et al., 2017; Schneider et al. 2016). The probabilistic approach used in this study allows for a more accurate identification of hazard zones based on varying exceedance probabilities. This method can be adapted to areas without probabilistic tsunami maps, segmenting regions according to these probabilistic criteria. For example, the black line in Fig. 11b could define evacuation zones, the blue line for critical infrastructure, and the red line for structures designed to withstand tsunami forces. Compared with existing strategies, such as Japan's Level 1 and Level 2 tsunami classifications (Shibayama et al. 2013), the proposed criteria offer flexibility and adaptability to diverse regional contexts, especially in areas like Chile and Peru with varying coastal topography. While this approach does not replace fully probabilistic tsunami maps, it provides a more accessible method for identifying tsunami risk areas in communal regulatory plans.

To better understand the impact of a 30-meter ground elevation as a tsunami inundation limit, we calculated the return periods and exceedance probabilities over a 50-year period for each location. We selected the transect line with the maximum runup at each location for our analysis, meaning that the computed return period for any other transect line within the same location would be longer. It is important to note that only one location, Iquique, reported a simulated runup exceeding 30 m. Therefore, we computed the empirical weighted distribution function and fitted a curve to extrapolate the required value, as illustrated in Fig. 13. In this figure, the continuous lines represent the empirical weighted functions, while the dashed line indicates the fitted function. It is possible to observe that the return periods for a 30-meter runup can easily exceed 100,000 years. The numerical values of return periods and exceedance probabilities are presented in Table 2. Notably, Talcahuano, located within Concepción Bay, shows extremely high return periods. This is not unexpected, since all simulated and recorded tsunami runup inside the bay do not exceed

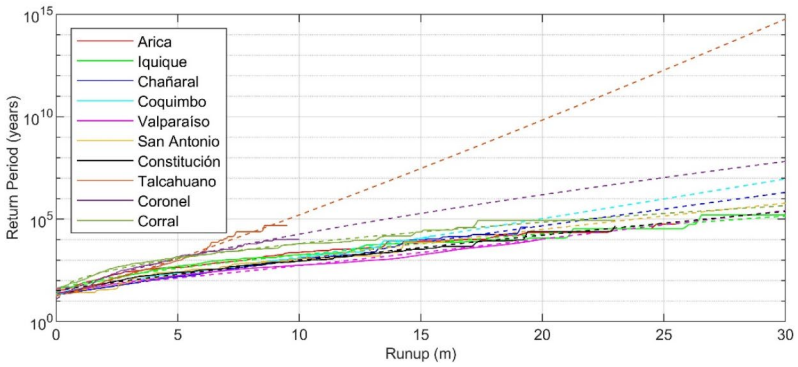

Fig. 13 Return period as a function of runup for a representative transect line in each location. The solid line represents the empirical curve, and the dashed line corresponds to the fitted curve

Table 2 Return periods and exceedance probabilities in 50 years period for a 30-m runup at each location

Coastal cities	Return period (years)	Exceedance probability (%) in 50 year period
Arica	149.300	0.033
Iquique	139.960	0.036
Chañaral	2.014.900	0.00248
Coquimbo – La Serena	9.147.600	0.000547
Valparaíso – Viña del Mar	263.540	0.019
San Antonio	604.340	0.00827
Constitución	237.580	0.021
Talcahuano	583.750.000.000.000	8.5×10^-10
Coronel	65.760.000	0.000076
Corral	454.950	0.011

9–10 m. Consequently, using a 30-meter ground elevation as a tsunami inundation limit may be excessively conservative.

While this study makes significant contributions to the identification of different tsunami risks areas and to the development of criteria based on probabilistic analysis in areas where no probabilistic maps are available, it is essential to acknowledge its limitations. Assumptions made during numerical simulations and uncertainties in historical data may introduce potential sources of error. Furthermore, it was found that probabilistic tsunami inundation is very sensitive to the *b*-value in the Gutenberg-Richter law (Aránguiz et al. 2024), which is related to the recurrence of seismic events. Nevertheless, the methodology used in the creation of the criteria provides results similar to those of probabilistic maps. The advantage of this methodology is that its results are much less computationally expensive compared to a probabilistic map and could be used in any location without the need to simulate new scenarios. To enhance the proposed method, the scenarios could be clustered by topographical features and new results could be obtained for runup and inundation distance based on a characterization of the cities under study.

5 Conclusions

The present research proposed new criteria for identification of tsunami inundation limits based on a probabilistic analysis of tsunami runup and inundation distance. These new criteria can be used as an input for tsunami hazard in communal regulatory plans and thus facilitate the definition of risk areas. The main conclusions are the following:

- The observed runup values in this study are consistent with historical tsunami events. Our findings not only corroborate these historical records but also extend our understanding by providing comprehensive runup-distance data in several locations along the Chile-Peru subduction zone.
- Two criteria were created based on probabilistic analysis; the blue-line criterion may be recommended for the location of critical infrastructure and the red-line criterion can be used to require that structures be designed to withstand tsunamis forces. However, any critical infrastructure must be designed to withstand tsunami forces.

- The current criterion based on the 30-m ground elevation could be very conservative if it is applied to urban planning or structure design requirements. Instead, the use of combined variables such as runup and inundation distance provides more representative results for the complex geomorphology of the Chilean coast.
- The proposed criteria can be used in communal regulatory plans to establish general tsunami inundation hazard levels to assess tsunami risk in a gradual manner.Therefore, areas without available probabilistic tsunami inundation maps may be segmented according to the current proposed criteria.

Acknowledgements This research was partially funded by ANID/FONDECYT grants 1210496 and 1210540. It was also partially supported by the supercomputing infrastructure of the NLHPC (ECM-02). R.A. also thanks the Research Center for Integrated Disaster Risk Management: ANID/ 1523A0009 FONDAP 2023 and the UCSC Office of Research for funding by means of FAA2023.

Data availability Tsunami source database and inundation maps are available at https://data.mendeley.com/datasets/b85kvbm8ht/2. Runup and inundation distance database is available upon request.

Declarations

Competing interests The authors declare no competing interests.

References

Adriano B, Mas E, Koshimura S, Fujii Y, Yauri S, Jimenez C, Yanagisawa H (2013) Tsunami inundation mapping in lima, for two tsunami source scenarios. J Disaster Res 8(2):274–284. https://doi.org/10.20965/jdr.2013.p0274

Alberniweather (2005) Port Alberni Tsunami Zone Map. https://www.alberniweather.ca/port-alberni-tsunami-zone-map/

Álvarez G, Quiroz M, León J, Cienfuegos R (2018) Identification and classification of urban micro-vulnerabilities in tsunami evacuation routes for the city of Iquique, Chile. Nat Hazards Earth Syst Sci 18(7):2027–2039. https://doi.org/10.5194/nhess-18-2027-2018

Aranguiz R, Shibayama T (2013) Effect of submarine canyons on tsunami propagation: a case study of the biobio canyon, Chile. Coastal Eng J 55(4). https://doi.org/10.1142/S0578563413500162

Aránguiz R, Catalán P (2022) Revisión De Los métodos de análisis de la amenaza de tsunami en Chile. In: Martínez C, Cienfuegos R, Barragán JM, Navarrete S, Hidalgo R, Arenas F, Fuentes L (eds) Hacia una ley de costas en Chile: bases para una gestión integrada de zonas costeras, 1st edn. Instituto de Geografia de la Pontificia Universidad Católica de Chile, pp 159–176

Aránguiz R, González G, González J, Catalán PA, Cienfuegos R, Yagi Y, Okuwaki R, Urra L, Contreras K, Del Rio I, Rojas C (2016) The 16 September 2015 Chile Tsunami from the Post-tsunami Survey and Numerical modeling perspectives. Pure appl Geophys 173(2):333–348. https://doi.org/10.1007/s00024-015-1225-4

Aránguiz R, Ramos M (2024) Stochastic tsunami source database along Chile subduction zone. In Mendeley Database. https://data.mendeley.com/datasets/b85kvbm8ht/1

Aránguiz R, Ramos M, Sepúlveda I, Villagra P (2024) A new generation of tsunami inundation maps of Chilean cities: tsunami source database and probabilistic hazard analysis. Coastal Eng J. https://doi.org/10.1080/21664250.2024.2326269. In Press

Aránguiz R, Urra L, Okuwaki R, Yagi Y (2018) Development and application of a tsunami fragility curve of the 2015 tsunami in Coquimbo, Chile, Nat. Hazards Earth Syst. Sci 18:2143–2160. https://doi.org/10.5194/nhess-18-2143-2018

ASCE (2022) Minimum Design loads and Associated Criteria for buildings and other structures. ASCE/SEI 7–22. American Society of Civil Engineers, Reston, VA, USA

Barrientos S (2018) The Seismic Network of Chile. Seismol Res Lett 89(2A):467–474. https://doi.org/10.1785/0220160195

Borrero JC, Synolakis CE, Fritz H (2006) Northern Sumatra field survey after the December 2004 great Sumatra earthquake and Indian Ocean tsunami. Earthq Spectra 22(SUPPL 3). https://doi.org/10.1193/1.2206793

Carvajal M, Cisternas M, Catalán PA (2017) Source of the 1730 Chilean earthquake from historical records: implications for the future tsunami hazard on the coast of Metropolitan Chile. J Geophys Research: Solid Earth 122(5):3648–3660. https://doi.org/10.1002/2017JB014063

Catalán PA, Aránguiz R, González G, Tomita T, Cienfuegos R, González J, Shrivastava MN, Kumagai K, Mokrani C, Cortés P, Gubler A (2015) The 1 April 2014 Pisagua tsunami: observations and modeling. Geophys Res Lett 42(8):2918–2925. https://doi.org/10.1002/2015GL063333

Charvet I, Eames I, Rossetto T (2013) New tsunami runup relationships based on long wave experiments. Ocean Model 69:79–92. https://doi.org/10.1016/j.ocemod.2013.05.009

Cho Y-S, Hwang H-S, Kim J-Y, Kwon H-H (2016) Development of Hazard Map with probable maximum tsunamis. J Coastal Res 75:1057–1061

Cortés P, Catalán PA, Aránguiz R, Bellotti G (2017) Tsunami and shelf resonance on the northern Chile coast. J Geophys Research: Oceans 122(9):7364–7379. https://doi.org/10.1002/2017JC012922

Cubelos C, Shyam Kularathna AHT, Valenzuela VPB, Iliopoulos N, Quiroz M, Yavar R, Henriquez P, Bacigalupe G, Onuki M, Mikami T, Cienfuegos R, Aranguiz R, Esteban M (2019) Understanding community-level flooding awareness in remote coastal towns in northern Chile through community mapping. Geosci (Switzerland) 9(7). https://doi.org/10.3390/geosciences9070279

Dauni P, Firdaus MD, Asfariani R, Saputra MIN, Hidayat AA, Zulfikar WB (2019) Implementation of Haversine formula for school location tracking. Journal of Physics: Conference Series, 1402(7). https://doi.org/10.1088/1742-6596/1402/7/077028

de CNAT CN (2021), January 15 T. Cartas de Inundación. https://www.dhn.mil.pe/cnat/cartas-inundacion

Fritz HM, Petroff CM, Catalán PA, Cienfuegos R, Winckler P, Kalligeris N, Weiss R, Barrientos SE, Meneses G, Valderas-Bermejo C, Ebeling C, Papadopoulos A, Contreras M, Almar R, Dominguez JC, Synolakis CE (2011) Field Survey of the 27 February 2010 Chile Tsunami. Pure appl Geophys 168(11):1989–2010. https://doi.org/10.1007/s00024-011-0283-5

Geist EL, Parsons T (2006) Probabilistic analysis of tsunami hazards. Nat Hazards 37(3):277–314. https://doi.org/10.1007/s11069-005-4646-z

Grezio A, Babeyko A, Baptista MA, Behrens J, Costa A, Davies G, Geist EL, Glimsdal S, González FI, Griffin J, Harbitz CB, LeVeque RJ, Lorito S, Løvholt F, Omira R, Mueller C, Paris R, Parsons T, Polet J, Thio HK (2017a) Probabilistic Tsunami Hazard Analysis: multiple sources and global applications. Reviews of Geophysics, vol 55. Blackwell Publishing Ltd, pp 1158–1198. 4 https://doi.org/10.1002/2017RG000579

Grezio A, Babeyko A, Baptista MA, Behrens J, Costa A, Davies G, Geist EL, Glimsdal S, González FI, Griffin J, Harbitz CB, LeVeque RJ, Lorito S, Løvholt F, Omira R, Mueller C, Paris R, Parsons T, Polet J, Thio HK (2017b) Probabilistic Tsunami Hazard Analysis: multiple sources and global applications. Rev Geophys 55(4):1158–1198. https://doi.org/10.1002/2017RG000579

Grigoriu M (2009) Reduced order models for random functions. Application to stochastic problems. Appl Math Model 33(1):161–175. https://doi.org/10.1016/j.apm.2007.10.023

Hayes GP, Moore GL, Portner DE, Hearne M, Flamme H, Furtney M, Smoczyk GM (2018) Slab2, a comprehensive subduction zone geometry model. Science 362(6410):58–61. https://doi.org/10.1126/science.aat4723

Ilustre Municipalidad Iquique (2019) PLAN COMUNAL DE EMERGENCIA IQUIQUE 2019

Ilustre Municipalidad Toltén (2017) REUNIÓN ORDINARIA N° 16

Instituto Nacional de Normalización (1996) NCh433 Of.96: earthquake resistant design of buildings (in Spanish). Instituto Nacional de Normalización (INN). Santiago, Chile

Instituto Nacional de Normalización (2015) NCh3363:2015: structural design - buildings in risk areas of flooding due tsunami or seiche. Instituto Nacional de Normalización (INN). Santiago, Chile

Intergovernmental Oceanographic Commission (2014) Tsunami, The Great Waves, Revised Edition. http://itic.ioc-unesco.org/index.php?option=com_content&view=article&id=1169&Itemid=1137&lang=en

Jarpa M (2015), January 4 Constitución tras 27/F: falta de definición de terrenos seguros retrasa construcción de futuro hospital - La Tercera. https://www.latercera.com/noticia/constitucion-tras-27f-falta-de-definicion-de-terrenos-seguros-retrasa-construccion-de-futuro-hospital/

Kramer SL (2014) Performance-based design methodologies for geotechnical earthquake engineering. Bull Earthq Eng 12(3):1049–1070. https://doi.org/10.1007/S10518-013-9484-X/METRICS

Kulikov EA, Rabinovich AB, Thomson RE (2005) Estimation of tsunami risk for the coasts of Peru and Northern Chile. Nat Hazards 35(2):185–209. https://doi.org/10.1007/S11069-004-4809-3/METRICS

Lagos R, Lafontaine M, Bonelli M, Boroscheck R, Guendelman T, Massone LM, Saragoni R, Rojas F, Yañez F (2020) The quest for resilience: the Chilean practice of seismic design for reinforced concrete buildings. Earthq Spectra 37(1):26–45

León J, March A (2014) Urban morphology as a tool for supporting tsunami rapid resilience.A case study of Talcahuano, Chile. Habitat Int 43:250–262. https://doi.org/10.1016/j.habitatint.2014.04.006

León J, Vicuña M, Gubler A (2019) Increasing tsunami risk through intensive urban densification in metropolitan areas: a longitudinal analysis in Viña Del Mar, Chile. Int J Disaster Risk Reduct 41. https://doi.org/10.1016/j.ijdrr.2019.101312

LeVeque RJ, Waagan K, González FI, Rim D, Lin G (2016) Generating Random Earthquake events for Probabilistic Tsunami Hazard Assessment. Pure appl Geophys 173(12):3671–3692. https://doi.org/10.1007/s00024-016-1357-1

Martínez C, Moris R, Quense J (2017) Valoración de las áreas de riesgo por tsunami y potencial de evacuación: propuestas para la reducción del riesgo de desastres a escala local. Pontificia Universidad Católica de Chile, Centro UC Políticas Públicas

Massone LM (2013) Fundamental principles of the reinforced concrete design code changes in Chile following the mw 8.8 earthquake in 2010. Eng Struct 56:1335–1345. https://doi.org/10.1016/j.engstruct.2013.07.013

MDS (2017) Manual de Escalas para la Cuantificación del Riesgo de Desastres de Proyectos de Infraestructura Pública. www.ministeriodesarrollosocial.gob.cl

Mikami T, Shibayama T, Esteban M, Takabatake T, Nakamura R, Nishida Y, Achiari H, Rusli, Marzuki AG, Marzuki MFH, Stolle J, Krautwald C, Robertson I, Aránguiz R, Ohira K (2019) Field Survey of the 2018 Sulawesi Tsunami: Inundation and Run-Up heights and damage to Coastal communities. Pure appl Geophys 176(8):3291–3304. https://doi.org/10.1007/s00024-019-02258-5

Ministerio de Salud (2019) GUÍA DE DISEÑO PARA ESTABLECIMIENTOS HOSPITALARIOS DE MEDIANA COMPLEJIDAD

Mori N, Takahashi T, Hamaura SE, Miyakawa K, Tanabe K, Tanaka K, Tanaka M, Watanabe T, Matsutomi H, Naoe K, Noumi T, Yamaguchi E, Ando S, Fujii Y, Kashima T, Okuda Y, Shibazaki B, Sakakiyama T, Matsuyama M, Suzuki T (2011) Nationwide post event survey and analysis of the 2011 Tohoku earthquake tsunami. Coastal Eng J 54(1). https://doi.org/10.1142/S0578563412500015

Morton RA, Gelfenbaum G, Buckley ML, Richmond BM (2011) Geological effects and implications of the 2010 tsunami along the central coast of Chile. Sed Geol 242(1–4):34–51. https://doi.org/10.1016/j.sedgeo.2011.09.004

Naim NNN, Mardi NH, Malek MA, Teh SY, Wil MA, Shuja AH, Ahmed AN (2021) Tsunami inundation maps for the northwest of Peninsular Malaysia and demarcation of affected electrical assets. Environ Monit Assess 193(7):405

National Centers for Environmental Information (NCEI), & World Data Service (WDS) (2023) Global historical tsunami database. Natl. Cent. for Environ. Inf., Boulder, Colo., https://doi.org/10.7289/v5*pn93h7*. (Accessed 27 October 2023)

National Tsunami Hazard Mitigation Program (US) (2001) Designing for Tsunamis. Seven Principles for Planning and Designing for Tsunami Hazards

Oficina Nacional de Emergencia del Ministerio del Interior, O (2014) Solicita pronunciamiento sobre situación de riesgo actual de Hospital de Constitución y opinión sobre eventual construcción de nuevo Hospital en la misma ubicación

Ogami T, Sugai T (2018) Effects of longitudinal valley slopes on runup of the 2011 Tohoku tsunami on the Sanriku Coast, northeastern Japan. Quatern Int 471:253–266. https://doi.org/10.1016/j.quaint.2017.12.042

Okada Y (1985) Surface deformation due to shear and tensile faults in a half-space. Bull Seismol Soc Am 75(4):1135–1154. https://doi.org/10.1785/BSSA0750041135

Orellana V (2023), July 10 Columna de Víctor Orellana: Lecciones de Constitución y Licantén - La Tercera. https://www.latercera.com/opinion/noticia/columna-de-victor-orellana-lecciones-de-constitucion-y-licanten/ZOT34NGW4JF5FNZPPQZY45SEII/

Pontificia Universidad Católica de Chile (2010) Estudio de riesgo de sismos y maremoto para comunas costeras de las regiones de O'higgins y del Maule

Prasetya DA, Nguyen PT, Faizullin R, Iswanto I, Armay EF (2020) Resolving the shortest path problem using the haversine algorithm. J Crit Reviews 7(1):62–64. https://doi.org/10.22159/jcr.07.01.11

Priest GR, Goldfinger C, Wang K, Witter RC, Zhang Y, Baptista AM (2010) Confidence levels for tsunami-inundation limits in northern Oregon inferred from a 10,000-year history of great earthquakes at the Cascadia subduction zone. Nat Hazards 54(1):27–73. https://doi.org/10.1007/S11069-009-9453-5/METRICS

Reese S, Bradley BA, Bind J, Smart G, Power W, Sturman J (2011) Empirical building fragilities from observed damage in the 2009 South Pacific tsunami. In Earth-Science Reviews (Vol. 107, Issues 1–2, pp. 156–173). https://doi.org/10.1016/j.earscirev.2011.01.009

Rey C (2020), July 18 Hospitales de Cauquenes, Parral y Constitución cuentan oficialmente con sus terrenos para iniciar su construcción el 2021 – www.cauquenesnet.cl.https://cauquenesnet.cl/2020/07/18/hospitales-de-cauquenes-parral-y-constitucion-cuentan-oficialmente-con-sus-terrenos-para-iniciar-su-construccion-el-2021/

Saillard M, Audin L, Rousset B, Avouac JP, Chlieh M, Hall SR, Husson L, Farber DL (2017) From the seismic cycle to long-term deformation: linking seismic coupling and quaternary coastal geomorphology along the Andean megathrust. Tectonics 36(2):241–256. https://doi.org/10.1002/2016TC004156

Schneider B, Hoffmann G, Reicherter K (2016) Scenario-based tsunami risk assessment using a static flooding approach and high-resolution digital elevation data: an example from Muscat in Oman. Glob Planet Change 139:183–194. https://doi.org/10.1016/j.gloplacha.2016.02.005

Sepúlveda I, Liu PLF, Grigoriu M, Pritchard M (2017) Tsunami hazard assessments with consideration of uncertain earthquake slip distribution and location. J Geophys Research: Solid Earth 122(9):7252–7271. https://doi.org/10.1002/2017JB014430

Sepúlveda I, Liu PLF, Grigoriu M (2019) Probabilistic Tsunami Hazard Assessment in South China Sea with consideration of Uncertain Earthquake characteristics. J Geophys Research: Solid Earth 124(1):658–688. https://doi.org/10.1029/2018JB016620

Shibayama T, Esteban M, Nistor I, Takagi H, Thao ND, Matsumaru R, Mikami T, Aranguiz R, Jayaratne R, Ohira K (2013) Classification of Tsunami and Evacuation Areas. Nat Hazards 67(2):365–386. https://doi.org/10.1007/S11069-013-0567-4/METRICS

Shimozono T, Sato S, Okayasu A, Tajima Y, Fritz HM, Liu H, Takagawa T (2012) Propagation and inundation characteristics of the 2011 Tohoku tsunami on the central Sanriku coast. Coastal Eng J 54(1). https://doi.org/10.1142/S0578563412500040

Smart GM, Crowley KHM, Lane EM (2016) Estimating tsunami run-up. Nat Hazards 80(3):1933–1947. https://doi.org/10.1007/s11069-015-2052-8

Solís IA, Gazmuri P (2017) Evaluation of the risk and the evacuation policy in the case of a tsunami in the city of Iquique, Chile. Nat Hazards 88(1):503–532. https://doi.org/10.1007/s11069-017-2876-5

Sucuoglu H, Akkar S (2014) Basic Earthquake Engineering, From Seismology to Analysis and Design. Springer, ISBN 978-3-319-01025-0, https://doi.org/10.1007/978-3-319-01026-7

Synolakis CE, Kong L (2006) Runup measurements of the December 2004 Indian Ocean tsunami. Earthq Spectra 22(SUPPL 3). https://doi.org/10.1193/1.2218371

Takahashi R (1961) A Summary Report on the Chilean Tsunami of May 1960. Report on the Chilean Tsunami of May 24, 1960, as observed along the Coast of Japan.

UNESCO, & IOC (2019) TSUNAMI GLOSSARY, 2019 (Fourth). Intergovernmental Oceanographic Commission of the United Nations Educational, Scientific and Cultural Organization. http://ioc.unesco.org

Van Den Berg I, Daals RJ, Heuberger CEM, Hildering SP, Van BE, Smulders MCM (2016) Tsunami impact analysis in Coquimbo Bay Multidisciplinary approach to mitigate future tsunami hazards. http://repository.tudelft.nl/

Vicuña M, Schuster JP (2021) Planificación urbana y gestión del riesgo de desastres: desafíos para instrumentos y mecanismos de planificación urbana y territorial (K. Campos, Ed.; 1st ed.). CIGIDEN

Widiyanto W, Hsiao SC, Chen WB, Santoso PB, Imananta RT, Lian WC (2020) Run-up, inundation, and sediment characteristics of the 22 December 2018 Sunda Strait tsunami, Indonesia. Nat Hazards Earth Syst Sci 20(4):933–946. https://doi.org/10.5194/nhess-20-933-2020

Yamazaki Y, Cheung KF (2011) Shelf resonance and impact of near-field tsunami generated by the 2010 Chile earthquake. Geophys Res Lett 38(12). https://doi.org/10.1029/2011GL047508

Yamazaki Y, Cheung KF, Kowalik Z (2011) Depth-integrated, non-hydrostatic model with grid nesting for tsunami generation, propagation, and run-up. Int J Numer Methods Fluids 67(12):2081–2107. https://doi.org/10.1002/fld.2485